CrystEngComm

RSCPublishing

ARTICLE

Intermolecular Hydrogen Transfer and Solubility Tuning in Multi-Component Molecular Crystals of the API Piroxicam

Cite this: DOI: 10.1039/xoxxoooooox

Received ooth January 2012,
Accepted ooth January 2012

DOI: 10.1039/xoxxoooooox

www.rsc.org/

Lynne H. Thomas,[a] Anneke R. Klapwijk,[a,b] Craig Wales[a,c] and Chick C. Wilson[a]*

A series of twelve multi-component molecular crystals of the active pharmaceutical ingredient (API) piroxicam (PX) have been synthesised and their structures analysed with respect to their supramolecular motifs and degree of intermolecular hydrogen transfer observed on formation of the various complexes. The multi-component crystals of PX formed with a series of basic N-heterocycles are contrasted with those formed with strong haloanilic acids, with PX found to adopt different ionisation states. The effect of the formation of these multi-component molecular crystals on the physical property of solubility, often crucial in API formulation, has been investigated and these solubility determinations are compared with those of the parent PX material. Enhanced solubility is evident in some of the multi-component crystals formed.

Introduction

Multi-component crystallisation – also referred to as co-crystallisation – is the method of bringing together two or more different molecules into the same crystal lattice to form a molecular complex or salt[1]. Molecular complexes from co-crystallisation experiments are seen as an increasingly useful tool in the preparation of solid forms of active pharmaceutical ingredients (APIs), with molecular complexes of pharmaceuticals not only having the potential to be patented as new materials[2], but also for improving the physicochemical properties of an API without compromising the structural integrity[3]. Piroxicam (PX) is a non-steroidal anti-inflammatory drug (NSAID) that has been extensively studied in the solid state[4-11]. Presented here are further investigations of multi-component molecular crystals of this important API, with particular regard to the crystal engineering potential and the potential modification of relevant physical properties of the multi-component crystals formed, with respect to those of the parent material. In terms of the crystal engineering aspects, the aim is to identify robust synthons which may be utilised for future design of molecular complexes of piroxicam, while the particular physical property under investigation here is that of solubility, relevant to a wide range of APIs in seeking to develop their optimized formulation in manufacturing and processing of pharmaceutical products.

In the solid state, piroxicam has previously been shown to exist in two ionisation states when not in its neutral form. While pure piroxicam exists in the non-ionised form in the solid state, it has been shown that in polar solvents, such as acetonitrile which is commonly used in crystallisation experiments with piroxicam, the zwitterionic form is present in large quantities[12,13]. The formation of the zwitterion, through intramolecular hydrogen-transfer, has been observed in solvates and multi-component molecular crystals of piroxicam[14] in almost equal numbers to molecular complexes including neutral piroxicam. On the other hand, intermolecular hydrogen transfer has been observed in only one piroxicam complex, with ethanolamine (1:1, pKa = 9.5), forming a salt with a piroxicam anion (PX^-)[15]. There is an ongoing debate as to nomenclature adopted in the case of neutral or ionic molecular complexes in this area; for convenience all such cases are generally referred to as multi-component molecular crystals in this work, while the ionisation state is clearly indicated.

The occurrence of such proton transfer is often rationalised by pKa matching[16], and the pKa rule[16-18], which includes the approximation that $\Delta pKa = pKa[base] - pKa[acid] \geq 3$ for salt formation[16]. This presents an interesting dilemma in attempting to apply the pKa rule to predict intermolecular hydrogen transfer in a potentially zwitterionic material such as piroxicam. The hydroxyl group of piroxicam has a pKa of 5.46, while that of the pyridine nitrogen is 1.86 (conjugate acid). The likelihood of proton transfer will be influenced, as expected, by the crystallisation solvent, but intramolecular hydrogen transfer is also influenced by the solvent and therefore pKa values may not be consistent as zwitterionic forms can exist. In the case of the piroxicam ethanolamine salt, intermolecular hydrogen transfer is successfully predicted by application of the pKa rule for hydrogen transfer[15]. However, in general the tendency of piroxicam to adopt the zwitterionic tautomer when co-

crystallised with weak acids must be taken into consideration when trying to predict hydrogen transfer.

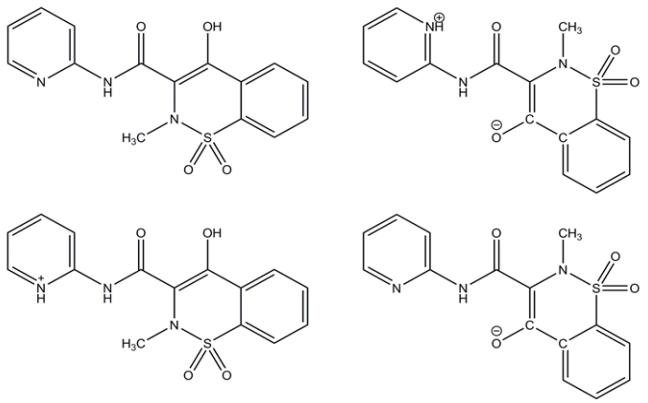

Figure 1. The different possible configurations for the piroxicam (PX) molecule. Top left, neutral PX with an intramolecular OH···O hydrogen bond. Top right, zwitterionic form of PX with a significant conformational change and two intramolecular NH···O hydrogen bonds. Bottom left, positively charged PX with an intramolecular O-H···O hydrogen bond and both N atoms protonated; the conformation of this molecule is the same as for neutral PX. Bottom right, negatively charged PX has a conformation similar to the zwitterionic form with a single intramolecular N-H···O hydrogen bond but with the pyridine ring rotated.

In the present work, intermolecular proton transfer from piroxicam is investigated in the formation of a series of multi-component molecular crystals. In the first approach, nitrogen heterocycles (NHCs) of varying basicity are co-crystallised with piroxicam to investigate the occurrence of hydrogen transfer from the piroxicam molecule to the basic nitrogen of the heterocycle and examine the effect of the competition of intramolecular hydrogen-transfer. In addition, the occurrence of the zwitterionic tautomer of piroxicam and the conditions which give rise to its formation in the solid state are investigated.

In addition to using basic NHCs, a series of multi-component molecular crystals formed when piroxicam is co-crystallised with the strong organic acids, chloranilic and bromanilic acid are reported. This is driven by the possibility of inducing protonation of the PX pyridine ring to form molecular salts in which piroxicam would be found in cationic form (PX^+).

An important target physical property in the study of molecular complexes of APIs is that of enhanced solubility (and hence potential delivery and bioavailability of the API). This property is also investigated here, by comparing solubilities of the parent API piroxicam, for which some previous literature determinations are avaialble[19,20], with those of the multi-component crystals formed in this study.

Experimental

Eight multi-component molecular crystals of PX with *N*-heterocyclic co-formers, and four with the strong chloro and bromo haloanilic acids were synthesised by multi-component evaporative crystallisation from 1:1 stoichiometric solutions of component starting materials, with either methanol or acetonitrile (ACN) as solvent. The crystal structures were determined by single crystal X-ray diffraction† and include both solvated and polymorphic forms; the materials synthesized and studied are summarised in Table 1.

In the cases of PX crystallization with imidazole and chloranilic acid, the product formed was found to vary with choice of solvent or crystallisation temperature. For the PX imidazole system different solvates were formed through crystallisation from methanol (**1**) and also for the pair of materials crystallised from ACN at RT (**2**) and 50°C (**3**), while for PX with chloranilic acid, crystallisation from ACN at RT produced one polymorph (form I; **9**), crystallisation at 40°C produced polymorphic form II (**10**), while crystallisation at 50°C produced a solvate (**11**). This variation illustrates the sensitivity of molecular complex formation to the crystallisation conditions used.

Single-crystal X-ray diffraction data were collected on **1-12** using either a Bruker Apex II (**1**, **2**, **4-6**, **9-12**) or a Bruker-Nonius Kappa CCD (**3**, **7**) diffractometer equipped with graphite monochromated Mo-Kα radiation (λ = 0.71073 Å), with the exception of those for **8**. The existence only of very small, weakly scattering, crystals led to data being collected for **8** on the I19 beamline at the Diamond Light Source, Harwell, UK, using an incident radiation of wavelength 0.6889 Å; in spite of the use of synchrotron radiation, the quality of data for **8** was rather poor. All data were collected at 100K. All structures were solved by direct methods using SHELXS-97[21] and refined using SHELXL-97[21] both within the WinGX program suite.[22] All non-hydrogen atoms were refined anisotropically. Treatment of the hydrogen atoms varied between the complexes studied, combining location of H atoms in difference Fourier maps, as detailed in the ESI. Complexes **3** and **6** showed evidence of disorder, which was modelled during the refinement, while the refinement of **8** was of rather poor quality and required the use of constraints due to the limited data available (see ESI).

Solubilities of starting material (PX form I) and a selection of product multi-component crystals (**1**, **2**, **4 9**, **10**) for which significant quantities of powdered samples could be prepared, were obtained using the Crystal16 parallel crystalliser from Avantium Technologies BV using turbidity probes on 1mL samples. Preliminary measurements of solubility were made in one or both of the solvents methanol and ethanol; attempts to measure in water were unsuccessful as on contact with water the complexes appeared to dissociate, with visual evidence (colour) that the co-former dissolved in the water and PXRD studies indicating the PX formed its monohydrate form as a residue on the surface of the water. Vials were cycled through various temperature ranges between 5°C and 75 °C using a temperature ramp rate of 0.5 °C min^{-1}, with bottom stirring at 850rpm using standard magnetic stirrer bars. Data were analysed using CrystalClear software version 1.0.1.614 supplied by Avantium Technologies BV. These turbidity measurements of solubility of PX in the multi-component crystals studied are preliminary; for API targets, more detailed studies would focus on solubility in water, which are initially difficult in this case as noted above. It should also be noted,

however, that for many molecular materials other than APIs, solubility in common solvents such as the simple alcohols is highly relevant and significant for function, and solubility measurements in media other than water are commonly employed in the development of new solid forms[23].

Table 1. Summary of multi-component molecular crystals including crystallization conditions and ionization state of the piroxicam molecule.

Complex	Co-former	Solvent	Crystallisation Temperature (°C)	Product complex
(**1**)	Imidazole (IM)	Methanol	RT	PX^{-} IM^{+} hemihydrate (2:2 :1)
(**2**)	Imidazole (IM)	Acetonitrile	RT	PX^{-} IM^{+} ACN solvate (1:1:1)
(**3**)	Imidazole (IM)	Acetonitrile	50	PX^{-} IM^{+} ACN solvate (4:4:1)
(**4**)	2-Methylimidazole (MIM)	Acetonitrile	RT/40/50	PX^{-} MIM^{+} (1:1)
(**5**)	Benzimidazole (BZ)	Acetonitrile	50	PX^{-} BZ^{+} (1:1)
(**6**)	1,2,4–Triazole (TA)	Acetonitrile	40/50	PXZ (zwitterionic) TA (1:1)
(**7**)	Benzotriazole (BT)	Acetonitrile	RT/40	PXZ BT (1:1)
(**8**)	Pyrazine*(PZ)	Acetonitrile	50	PXZ PZ (2:1)
(**9**)	Chloranilic acid (CA)	Acetonitrile	RT	PX^{+} CA^{-} (1:1) form I
(**10**)	Chloranilic acid (CA)	Acetonitrile	40	PX^{+} CA^{-} (1:1) form II
(**11**)	Chloranilic acid (CA)	Acetonitrile	50	PX^{+} CA^{2-} ACN solvate (2: 1: 2)
(**12**)	Bromanilic acid (BA)	Acetonitrile	RT/40/50	PX^{+} BA^{-} (1:1)

* Production of the PXZ:PZ complex was found to result only from a small minority of the preparations set up with these starting materials, and in small yield overall. In addition, the resulting single crystals were small, and data were collected using synchrotron radiation.

Results and Discussion

Piroxicam Conformation

The protonation state of the piroxicam molecule can clearly be inferred not just from the identification of hydrogen atoms in Fourier difference maps, but also by the conformation of the molecule itself (Figure 1). A significant molecular rearrangement accompanies the conversion of the neutral piroxicam molecule to its zwitterionic form.[9] In the neutral piroxicam molecule, an intramolecular OH···O hydrogen bond is formed. On conversion to the zwitterionic form, this hydrogen atom is transferred to the N atom of the pyridine ring and instead two NH···O charge assisted intramolecular hydrogen bonds are formed. When the piroxicam molecule is protonated (PX^{+}), both N atoms and the hydroxyl group O atom are protonated; the molecule in this case shows a preference for an intramolecular OH···O hydrogen bond and overall the molecule adopts a similar conformation to the neutral molecule (**9-12**; Figure 1, bottom left). In contrast, the deprotonated piroxicam molecule (PX^{-}) is always deprotonated at the hydroxyl group and thus adopts a configuration similar to the zwitterionic form, this time with only a single intramolecular NH···O hydrogen bond and therefore the pyridine ring is rotated when compared to the zwitterionic form (**1-5**; Figure 1, bottom right). The piroxicam molecule therefore modifies its conformation in order to maximise the number of intramolecular hydrogen bonds in every case.

Multi-component Molecular Crystals of Piroxicam with N-heterocycles

Of the eight PX complexes (for convenience, the shorthand "complexes" is adopted as a shorthand nomenclature for the term multi-component molecular crystals in some of the discussion below) with NHCs, transfer of the PX hydroxyl hydrogen to the NHC to form the deprotonated PX^{-} occurs in five (**1-5**). Three of these are solvated complexes with imidazole (IM), which all feature protonation of the IM. The other three complexes (**6-8**) feature intramolecular hydrogen transfer within the PX molecule and form zwitterionic piroxicam (PXZ). Hydrogen transfer is a consistent feature in these multi-component molecular crystals, with none containing the non-ionised form of piroxicam (PXN). The conformation of the PX molecules is thus similar in all of the complexes with NHCs.

All PX^{-} complexes feature chains of alternating PX^{-} and NHC, with an ABAB arrangement. They also exhibit similar hydrogen bonding synthons, although with some noticeable differences. Complexes **2-5** feature NHC molecules sandwiched between two PX^{-} molecules and linked by NH···O=C hydrogen bonds to the PX^{-} amide oxygen and NH···O^{-} hydrogen bonds to the PX^{-} enolate oxygen (Figure 2; geometrical parameters of hydrogen bonds are given in the ESI). Complex **1** contrasts to these as neither of the two independent IM^{+} molecules follow this hydrogen bonding pattern despite also having an ABAB arrangement (Figure 3). Instead, one chain features hydrogen bonds from the IM^{+} NH groups to the PX^{-} pyridine nitrogen and enolate oxygen, and the other chain has both NH groups hydrogen bonding to the PX^{-} amide oxygen atoms. One enolate oxygen atom of PX^{-} is therefore not hydrogen bonded to the IM^{+} NH groups and instead forms a hydrogen bond to the IM^{+} CH in the 4/5 position. Other IM^{+} CH groups in the 4 and 5 positions in the structure form hydrogen bonds with either the PX^{-} pyridine nitrogen or a sulfonyl oxygen atom.

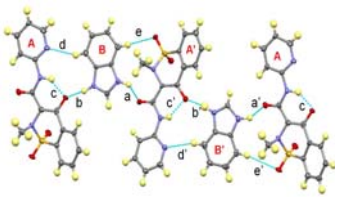

Figure 2. Hydrogen bonding in the ABAB chains in complex **5** (the dashes ' indicate a symmetry independent molecule or interaction e.g. A and A'). The same hydrogen bonding pattern is found in **2**-**4**. Hydrogen bonds denoted by letters, in this and subsequent figures, are fully specified in the ESI.

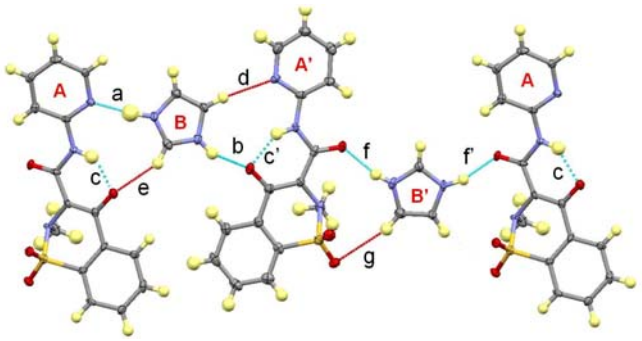

Figure 3. Hydrogen bonding in the chains of PX^- and IM^+ in complex **1** (those marked with ' indicate a symmetry independent molecule or interaction e.g. A and A'). One IM^+ molecule forms both NH···N and NH···O hydrogen bonds (blue dashed lines from B) and the other forms two NH···O hydrogen bonds (blue dashed lines from B'). Weaker hydrogen bonds involving CH donors are shown as red dashed lines.

Weak hydrogen bonds are also seen in the other PX^- structures, with CH···N interactions occurring in the imidazole acetonitrile solvate complexes **2** and **3** (d and d' in Figure 6 below), as well as with the analogous CH groups in the 5/8 positions of BZ^+ in **5** (d and d' in Figure 2). Complex **4** does not have this interaction due to the alternate PX^- molecules lying head to head rather than head to tail which makes the pyridine nitrogen unavailable for hydrogen bonding to the MIM^+ CH groups (Figure 4). A CH···O=S interaction is present in complexes **4** and **5** (5/8 position; e and e' in Figure 2) but not in either of the imidazole ACN solvates **2** and **3**. In **2**, the lack of interaction is compensated for by a CH hydrogen bond forming to the ACN nitrogen, with the ACN methyl group then forming a CH···O=S hydrogen bond to the PX^- molecule (Figure 5). A similar CH···N hydrogen bond to the ACN is formed in **3**, although no CH···O=S interaction is formed between the ACN and PX^- as the ACN methyl group points away from the sulfonyl oxygen (Figure 6).

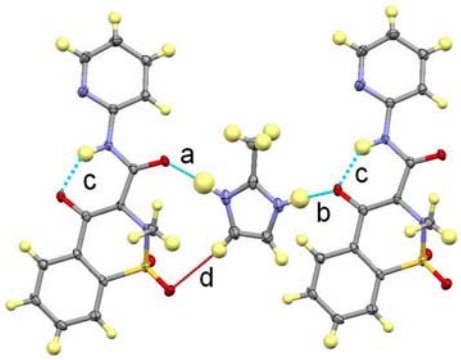

Figure 4. NH···O^- and NH···O hydrogen bonds (blue dashed lines) between PX^- and $2MIM^+$ and the weak CH···O hydrogen bond (red dashed line), in the molecular salt complex **4**. The molecules lie head to head and this arrangement means that there are no CH···N weak hydrogen bonds formed.

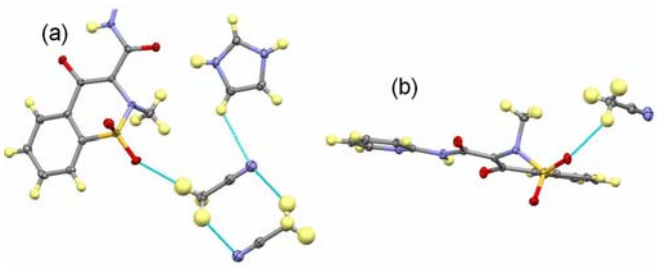

Figure 5. Weak hydrogen bonds involving the ACN molecule in **2**. (a) Weak CH···O and CH···N hydrogen bonds linking ACN molecules into the chains and weak CH···N hydrogen bonds resulting in ACN dimers. (b) Weak CH···O hydrogen bond between the ACN molecule and the PX^- molecule in the chain below.

It is worthy of note that despite the similarity in hydrogen bonding arrangements between the IM^+ complexes **1**-**3** and those of MIM^+ (**4**) and BZ^+ (**5**), no non-solvated multi-component molecular crystals of PX and IM could be isolated, with instead two ACN solvates and a hydrate produced from varying the conditions. This is likely due to the small size of IM compared with BZ and MIM, which both have bulky groups attached to the imidazole group. To compensate for the void that would be left and to ensure efficient packing in the absence of these groups, a solvent molecule is incorporated into the PX^-:IM+ complexes. This is reflected in the relative positions of the H_2O and ACN molecules in **1**-**3**, as the H_2O molecule is hydrogen bonded to the CH group in the 2-position and the ACN molecules form hydrogen bonds to the CH in the 4/5 position. The solvent molecules therefore occupy equivalent positions to that adopted by methyl group and benzene ring in the complexes containing 2MIM (**4**) and BZ (**5**), respectively.

In the three complexes featuring the zwitterionic PXZ with NHCs (**6**-**8**), the PXZ molecules dimerise, consistent with previously reported PXZ complexes[9]. With the exception of the pyridinium nitrogen which is involved in hydrogen bonding to form the PXZ dimer, consistent hydrogen bonding is observed between the strongest *N*-heterocycle donors and the strongest free PXZ acceptors in all cases (Figures 7 and 8). In **6** and **7**, NH···O^- hydrogen bonds are formed between the TA/BT NH and the enolate oxygen (d in Figures 7 and 8). The PZ CH also forms hydrogen bonds to the enolate O^- (**8**). In all

complexes a hydrogen bond is also formed from the same CH group of the PX^{-} pyridine ring to a nitrogen atom of the heterocycles (e in Figures 7 and 8).

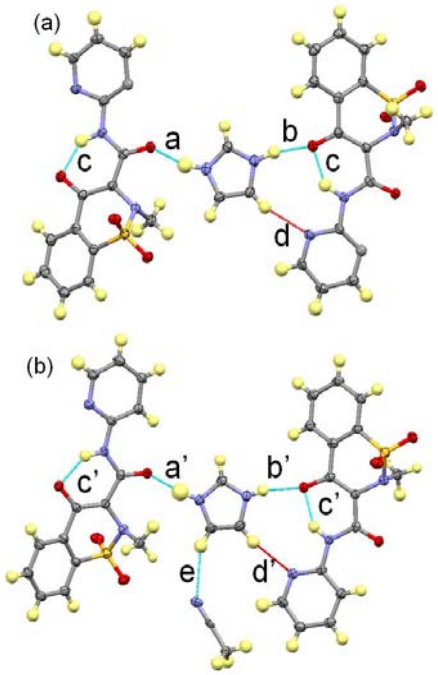

Figure 6. Hydrogen bonding in the symmetry independent chains of PX^{-} and IM^{+} molecules in **3**.

The PXZ:PZ complex **8** is unusual as the only hydrogen bonds between PZ and PXZ molecules involve CH donors, as this is the only possible PZ donor and the pyridinium nitrogen is unavailable due to dimerisation of PXZ molecules. The fact that no conventional hydrogen bonds occur between the molecules may explain why crystallisation of this complex occurs so rarely and in such small quantities. As PZ is symmetrical, the same interactions are formed on both sides of the molecule and it therefore forms chains with a BAABAAB configuration, with the PXZ dimers sandwiched by two PZ molecules and resulting in a 2:1 (PXZ:PZ) complex.

In the PXZ:TA complex (**6**), disorder of the TA molecule means it can effectively form the same interactions on both sides (therefore it shows no preference for each orientation; the disorder is 50:50 over an inversion centre for the two independent TA molecules) and therefore also forms a 2:1 complex of BAABAAB chains (Figure 7). The small size of the molecule allows it to occupy two possible positions without major disruption of the crystal packing. The PXZ:BT complex (**7**), however, forms a 1:1 complex with tetramers of BZT:PXZ:PXZ:BZT (BAAB; Figure 8, analogous to the common tetramer found in PXZ complexes with benzoic acids[9]. Chains are not formed as there is no symmetry in the BT molecule and only one sufficiently strong donor to form hydrogen bonds to the enolate O^{-}.

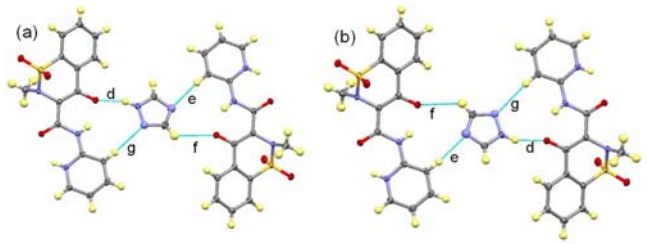

Figure 7. (a) The hydrogen bonding between TA molecules and PXZ molecules in **6**, with (b) showing the same interactions formed in reverse when the TA molecule is in its second orientation (50:50 orientational disorder).

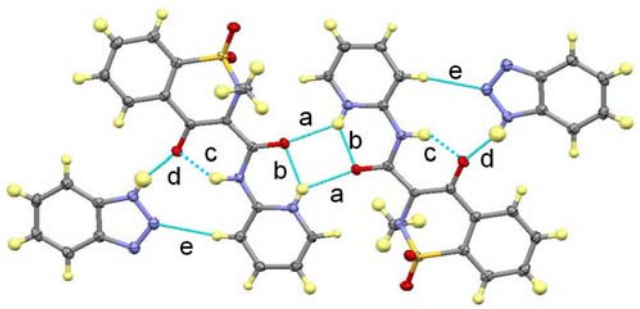

Figure 8. Hydrogen bonding in the PXZ:BT complex, **7**, forming a BAAB tetramer.

Multi-component Molecular Crystals of Piroxicam with Strong Acids: Chloranilic Acid and Bromanilic Acid

All multi-component molecular crystals of PX with CA and BA resulted in intermolecular hydrogen transfer from the CA/BA to the PX pyridine ring, forming the protonated PX^{+}; the first time this ionic form of PX has been isolated in the solid state. It adopts the same conformation as is seen in the non-ionised form of PX, with a short strong intramolecular OH···O hydrogen bond. The CA/BA molecules are strong acids with two acidic OH groups; it is therefore possible to form both the singly charged anion and the doubly charged anion depending on the stoichiometry of the two components in a molecular complex. In all these multi-component molecular crystals the strongest donor/strongest acceptor rule is satisfied, with charge-assisted hydrogen bonds formed between the protonated pyridine nitrogen of PX^{+} and the deprotonated oxygen of CA^{-} (or CA^{2-}).

The polymorphic PX^{+}:CA^{-} forms I (**9**) and II (**10**) both crystallise in a 1:1 ratio, under different conditions but both from acetonitrile as the solvent (form I room temperature; form II 40°C). Whilst bifurcated hydrogen bonds again form between the NH^{+} group of PX^{+} and the deprotonated part of CA^{-}, there is a significant change in orientation of the CA^{-} relative to the PX^{+} molecule between the two forms. The two components (PX^{+} and CA^{-}) are more co-planar in form I (**9**) (rotation of ~20.9° between the plane of the PX^{+} pyridine ring and the plane of the CA^{-} six-membered ring) and twisted by ~81.4° in form II (**10**) (Figure 9). This results in significantly different crystal packing (Figure 10). In form I, homodimers of CA^{-} are formed through the remaining OH group to form hydrogen bonded rings; these form isolated ABBA synthons with two CA^{-} molecules sandwiched by PX^{+} molecules (Figure

10, top). In form II, the hydroxyl group forms an intermolecular hydrogen bond to a sulfonyl O atom on a PX^+ molecule; these then assemble into hydrogen bonded chains in an ABAB arrangement contrasting to form I (Figure 10, bottom).

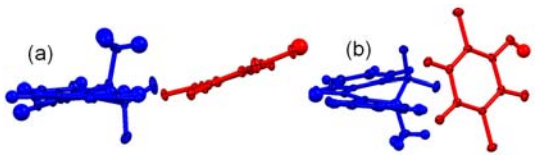

Figure 9. Relative arrangements of the PX^+ (blue) and CA^- (red) molecules in polymorphs **9** (a) and **10** (b), viewed along the pyridine ring plane. The CA^- molecule is significantly twisted in form 2 (**10**) and more co-planar in form 1 (**9**).

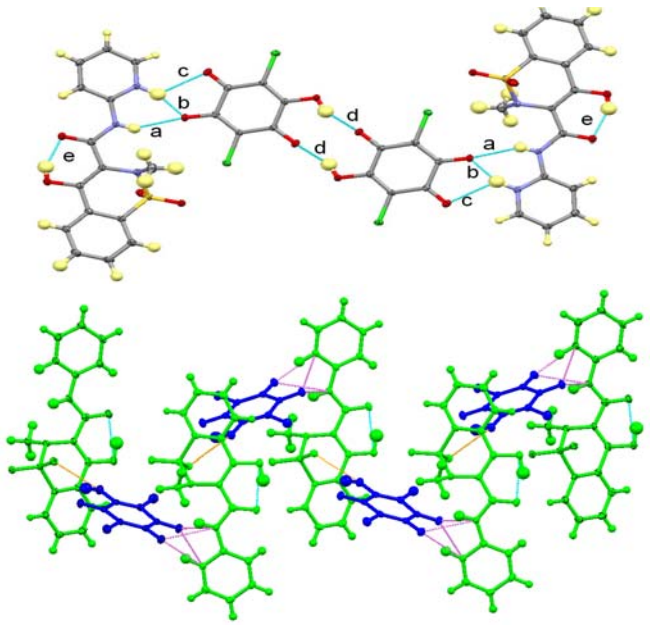

Figure 10. Tetrameric ABBA unit formed between the PX and CA molecules in the PX^+:CA^- form I (**9**; top), contrasted with the arrangement in form II (**10**; bottom), in which the CA molecules no longer dimerise through their OH group (bottom left), instead the latter form moderately strong OH···O interactions with the sulfonyl oxygen of another PX^+ molecule (orange dashed lines, bottom) and assemble into chains through bifurcated hydrogen bonds (pink dashed lines, bottom). Chloranilic acid in blue, piroxicam in green..

There are also halogen interactions involving the Cl atom. In form I, there are two C-H···Cl weak hydrogen bonds from aromatic CH groups on PX^+ molecules and a Cl···O interaction with a sulfonyl O atom; in form II, there is only one interaction per Cl atom, one C-H···Cl weak hydrogen bond from a methyl group on a PX^+ molecule and a Cl···π interaction to the fused benzene ring of a second PX^+ molecule. Since it is formed at a higher temperature of crystallisation and has lower density, form II is assumed to be the kinetic product.

Increasing the crystallisation temperature again to 50°C resulted in the ACN solvate complex **11**, with double deprotonation of the CA molecule and a 2:1 relative stoichiometry of PZ^+:CA^{2-} (Figure 11); this creates an ABA type supramolecular arrangement. Deprotonation of both OH groups of the CA molecule is somewhat expected due to the decrease in pKa associated with increasing temperature but the fact that the relative orientation of the PX and CA components is more similar to that of the low temperature polymorphic form **9** is not necessarily what would be expected as one might expect the product to be more similar to the kinetic form II than the thermodynamic form I; they are, however, not directly comparable due to the different ionization states of the CA.

The PX^+:BA^- complex (**12**) is isostructural to the PX^+:CA^- form II complex, while it might be expected to be isostructural to the more thermodynamically stable form I. Unlike the PX:CA complexes, only a single PX^+:BA^- phase was produced regardless of the temperature at which the crystallisation was carried out.

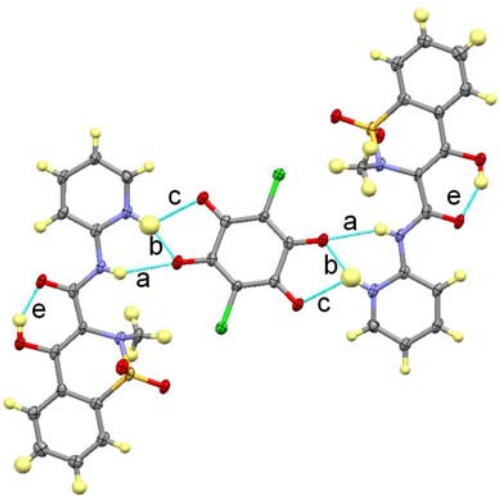

Figure 11. Hydrogen bonding between CA^{2-} and PX^+ molecules forming the ABA motif in **11**.

Hydrogen Transfer and pKa – the complications of Zwitterionic forms

Five of the eight multi-component molecular crystals of PX with *N*-heterocycles feature hydrogen transfer from the PX molecule to the basic nitrogen of the *N*-heterocycle; these represent the three most basic co-formers, all three IM complexes (**1**-**3**), the MIM complex (**4**) and the BZ complex (**5**). The ΔpKa values sit in the ΔpKa continuum region (see Table 2) and the value for benzimidazole is very close to zero and so proton transfer might not be expected. However, the pKa values will have been determined in water and it may be that in acetonitrile, a greater proportion of molecules are in the zwitterionic form and a pKa value for this would be more realistic; this would be consistent with the structural picture where the PX^- molecules adopt a conformation most similar to the zwitterionic form of PX. The remaining three co-formers are poorly basic and resulted in multi-component molecular crystals with the zwitterionic PX tautomer (**6**-**8**). The ΔpKa values show that the TA, BZ and PZ complexes would not be expected to result in intermolecular hydrogen transfer as they are all negative or very small; the pKa values for these co-formers are consistent with the pKa boundaries suggested by Wales *et al*[9] (all over 4) for a preference for the zwitterionic form. The ΔpKa values (where PX acts as the conjugate base)

for the CA and BA complexes fall in the continuum region, but again, there may be differences dependent on whether the piroxicam molecule is in its neutral or zwitterionic forms in the solution. With systems in which zwitterionic forms are possible, the application of the simple ΔpKa rule is likely to be less reliable than in other cases.

Table 2. The ΔpK_a values for piroxicam and co-molecules.

Co-former	pKa of co-former	PX Form	ΔpK_a OH (pK_a = 5.46)	ΔpK_a N^+-H (pK_a = 1.86)
		Bases		
Imidazole	6.99	PX^-	1.53	-
2-methylimidazole	7.88	PX^-	2.42	-
Benzimidazole	5.53	PX^-	0.07	-
1,2,4-triazole	2.27	PXZ	-3.19	-
Benzotriazole	1.60	PXZ	-3.86	-
Pyrazine	0.65	PXZ	-4.48	-
		Acids		
Chloranilic Acid	0.76	PX^+	-	1.1
Bromanilic Acid	0.7	PX^+	-	1.16

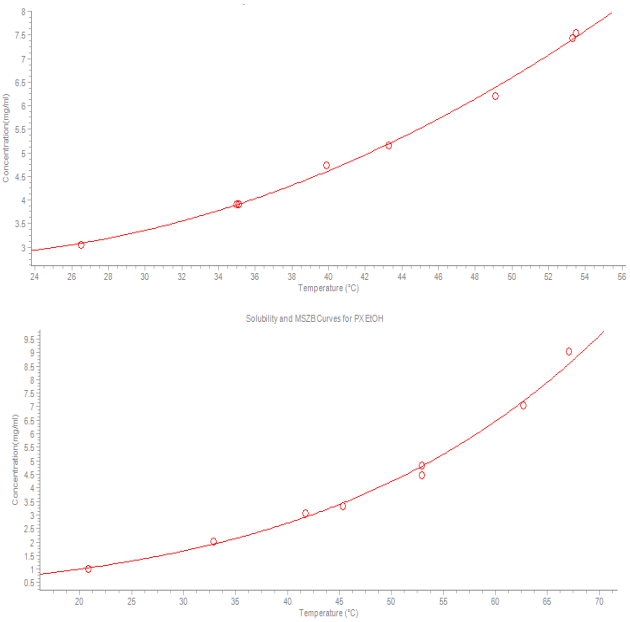

Figure 12. PX solubility curve in methanol (top) and ethanol (bottom).

Solubility of Multi-component Molecular Crystals of PX

The solubilities of the parent API piroxicam and of the w/w PX component of a series of the multi-component molecular crystals discussed above can be compared, to indicate whether formation of the multi-component crystal is found to increase or decrease the solubility of PX, a physical property vital for the potential delivery and bioavailability of such APIs. The solubility curves of PX (form I) in methanol and ethanol were determined, with values determined for the latter found to be consistent with previous literature reports of PX solubility[19,20]. The curves are similar in shape, with PX less soluble in ethanol throughout the temperature range (Figure 12). It should be noted that in the present study, no attempt has been made fully to characterise the degree of dissociation of the multi-component crystal into its individual components in solution; this will be pursued in future work using *in situ* process analytical tools.

Enhancement of the solubility is found for most of the multi-component molecular crystals of PX measured to date, for example for **1** in methanol (5.0 mg/ml w/w PX at 30°C; enhanced from the value of 3.1 mg/ml for pure PX) and for **4** in methanol (9.0 mg/ml PX at 30°C) (Figure 13). The solubility curves for **2** methanol and ethanol (see ESI) show less pronounced enhancement of solubility, with values (at 30°C) of ~4.0 and 1.6 mg/ml, respectively. Thus the solubility of PX in these multi-component molecular crystals, in which PX adopts its ionised PX^- form, is enhanced compared with that of the parent PX for these solvents.

For the PX CA complex **10**, in contrast, there appears to be a reduction in the measured w/w PX solubility in both methanol and ethanol (see ESI), also found for the polymorph complex **9** solubility in methanol. For these multi-component molecular crystals containing PX^+ there is thus a reduction in solubility on formation of the multi-component material.

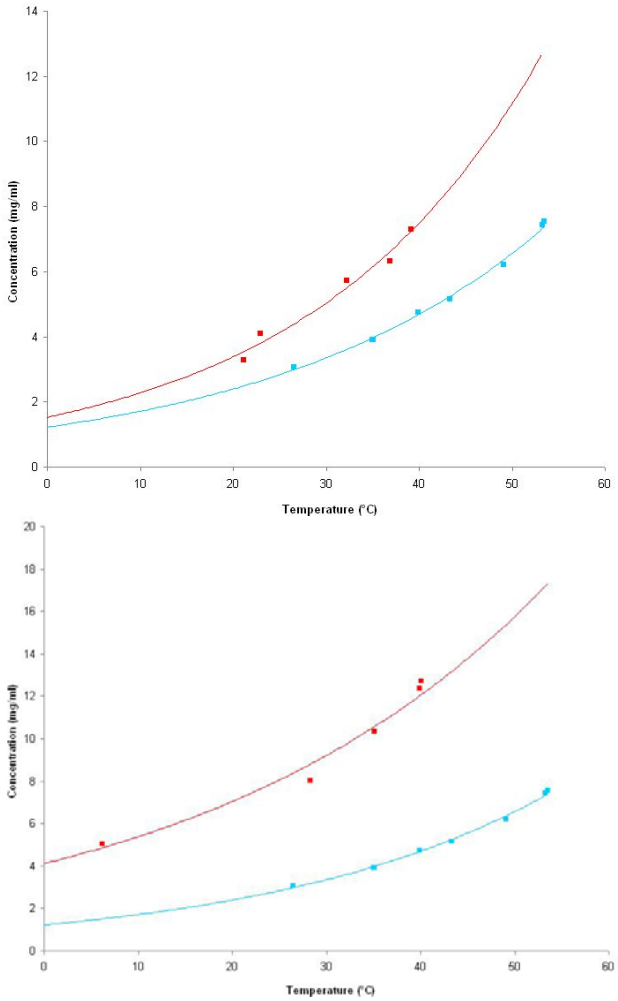

Figure 13. Solubility curves for w/w PX component (red) in complex **1** in methanol (top) and complex **4** in methanol (bottom), compared with the pure PX solubility curves (blue).

Conclusions

Eight multi-component molecular crystals of PX with NHCs have been formed and characterized. The three poorly basic NHCs (pKa = 0.65 - 2.27) resulted in the formation of multi-component crystals containing the zwitterionic PXZ form (**6-8**), with no intermolecular hydrogen transfer. All exhibited the dimerisation of the PXZ molecules seen in all known complexes featuring PXZ, with the strongest hydrogen bond donor of the NHC interacting with the enolate oxygen. In the case of PZ and TA this leads to the formation of infinite chains due to the symmetry in PZ and the disorder of TA which allow the same NH···O^- and CH···O^- interactions to form on both sides of the molecules. In the case of BT, discrete hydrogen bonded tetramers are formed as the NH donor of BT only lies on one side. The BT:PXZ:PXZ:BT tetramers are analogous to the BZZB tetramers formed in the zwitterionic PXZ complexes with benzoic acids[9].

Tuning of the pKa values of the co-former allows multi-component molecular crystals to be formed containing the PX^- anion. In this way, five complexes were crystallised featuring PX^- by using bases with pKa values in the range 5.33-6.99. All PX^- complexes exhibit consistent hydrogen bonding synthons, with interactions of the strongest donors and strongest acceptors (NH···O and NH···O^-) prevailing in all complexes except **1**. All PX^- complexes contain chains with a general ABAB arrangement of the molecules.

The three complexes (**1-3**) with PX^-:IM^+ include a hemihydrate as well as 1:1:1 and 4:4:1 ACN solvates. No non-solvated PX^-:IM^+ complex could be formed despite varying the crystallisation conditions. Selective crystallisation of the three PX^-:IM^+ solvates could be controlled by varying the crystallisation temperature.

Analysis of the ΔpKa values for the basic co-formers are in general agreement with the ΔpKa rule, but the situation may be more complex when PX exists in zwitterionic form. pKa values are generally measured using water as the solvent and in cases where zwitterionic forms are present, the transferability to different solvents may be less reliable..

Multi-component molecular crystals of CA and BA with PX resulted in salts where PX is present as a cation (PX^+) with both the hydroxyl and pyridinium N protonated (**9-12**). This is the first time PX has been seen in the PX^+ form. Polymorphism of the 1:1 CA:PX complex can be induced by changing the crystallisation temperature. Both forms have the same basic hydrogen bonding motif linking pairs of PX and CA molecules, but the CA^- molecule in form II is twisted relative to its position in form I, forming an extra hydrogen bond to a further PX^+ molecule rather than dimerising with another CA^- molecule. A further increase in temperature resulted in the production of a 2:1:2 ACN solvate which, perhaps surprisingly, reverts back to the motif seen in form I. .

Significant solubility enhancements are found for some of the multi-component molecular crystals for which this physical property has been determined to date, and this is potentially significant for the aim of enhancing this physical property in multi-component crystals of this, and other, APIs. However, the limited data available to date do not allow for possible correlations with PX ionisation states or with crystal packing to be drawn out fully; only a limited subset of ionic PX complexes have been characterised of which some show significantly enhanced solubility in the solvent used compared to pure PX. This will be pursued in further work related to the further investigation of crystallisation control of molecular complexes of APIs and enhancing their physical properties.

Acknowledgements

This work was supported by the Scottish Funding Council SPIRIT scheme, and as part of the EPSRC Centre for Innovative Manufacturing in Continuous Manufacturing and Crystallisation (CMAC), under grant EP/I033459/1. We thank Diamond Light Source for the provision of beamtime on I19. The authors would like to thank Dr Thomas McGlone (CMAC, University of Strathclyde) for assistance with solubility measurements.

Table 3. Summary of Crystallographic Data for **1**-**6**.

	1	**2**	**3**	**4**	**5**	**6**
Formula	$2(C_{15}H_{12}N_3O_4S)^-$, $2(C_3H_5N_2)^+$, H_2O	$(C_{15}H_{12}N_3O_4S)^-$, $(C_3H_5N_2)^+$, (C_2H_3N)	$4(C_{15}H_{12}N_3O_4S)^-$, $4(C_3H_5N_2)^+$, (C_2H_3N)	$(C_{15}H_{12}N_3O_4S)^-$, $(C_4H_7N_2)^+$	$(C_{15}H_{12}N_3O_4S)^-$, $(C_7H_7N_2)^+$	$2(C_{15}H_{13}N_3O_4S)$, $(C_2H_3N_3)$
M/g mol^{-1}	816.89	440.48	1638.78	413.46	449.48	731.76
T/K	100	100	100	100	100	100
Crystal System	Triclinic	Monoclinic	Monoclinic	Monoclinic	Triclinic	Triclinic
Space Group	P-1	$P2_1/c$	$P2_1/n$	$P2_1/n$	P-1	P-1
a/Å	6.8019(4)	8.1510(5)	6.9103(1)	10.9928(8)	12.005(3)	6.9267(2)
b/Å	14.4384 (8)	26.5997(17)	22.1444(5)	15.3135(15)	13.789(3)	8.3356(3)
c/Å	19.8727(12)	10.1579(7)	25.1813(5)	12.551(1)	13.810(4)	28.8177(10)
α	90.460(2)	90	90	90	72.186(7)	86.485(2)
β	99.276(2)	113.394(3)	97.068(1)	112.039(4)	68.682(7)	84.209(2)
γ	101.460(2)	90	90	90	80.962(7)	76.271(1)
V/Å^3	1886.1(2)	2021.3(2)	3824.07(13)	1958.4(3)	2024.8(8)	1606.89(9)
Z	2	4	2	4	4	2
ρ_{cal}/ g cm^{-3}	1.438	1.447	1.423	1.402	1.474	1.512
μ/mm^{-1}	0.211	0.202	0.207	0.202	0.202	0.235
θ Range/°	1.44 - 23.51	1.53 - 29.61	1.63 - 27.08	2.11 - 28.31	1.55 - 23.91	0.71 – 25.00
Ref. (meas. / ind.)	39251/ 5468	31169/ 5639	55396/ 8406	22181/ 4828	23716/ 6114	35311/ 7358
Observed>2σ	2890	4386	4565	3085	2700	5437
Rint	0.1704	0.1084	0.1572	0.1100	0.1716	0.0857
Completeness %	97.6	99.0	99.9	99.1	97.1	99.9
Parameters	538	294	592	327	597	503
GooF	0.949	1.146	0.978	0.985	0.887	1.096
R_1 (obs)	0.0567	0.0601	0.0572	0.0567	0.0618	0.0616
R_1 (all)	0.1543	0.0798	0.1322	0.1021	0.1858	0.0916
wR2 (all)	0.0996	0.1699	0.1456	0.1309	0.102	0.1327
$\rho_{max,min}$/e Å^{-3}	0.334, -0.327	0.594, -0.594	0.327, -0.389	0.519, -0.373	0.331, -0.339	0.544, -0.457

Table 4. Summary of crystallographic data for **7-12**.

	7	**8**	**9**	**10**	**11**	**12**
Formula	$(C_{15}H_{13}N_3O_4S)$, $(C_6H_5N_3)$	$2(C_{15}H_{13}N_3O_4S)$, $(C_4H_4N_2)$	$(C_{15}H_{14}N_3O_4S)^+$, $(C_6HCl_2O_4)^-$	$(C_{15}H_{14}N_3O_4S)^+$, $(C_6HCl_2O_4)^-$	$(C_{15}H_{14}N_3O_4S)^+$, $[0.5(C_6Cl_2O_4)]^-$, (C_2H_3N)	$(C_{15}H_{14}N_3O_4S)^+$, $(C_6HBr_2O_4)^-$
M/g mol^{-1}	450.47	742.80	540.32	540.32	476.89	629.24
T/K	100	100	100	100	100	100
Crystal System	Monoclinic	Triclinic	Triclinic	Monoclinic	Triclinic	Monoclinic
Space Group	$P2_1/c$	P-1	P-1	$P2_1/c$	P-1	$P2_1/c$
a/Å	11.6101(6)	6.792(11)	9.1504(4)	8.5627(5)	7.0616(8)	8.842(2)
b/Å	26.2908(15)	8.646(15)	10.9678(4)	13.3395(7)	11.6031(13)	13.437(2)
c/Å	6.7710(3)	29.66(5)	11.7747(5)	19.3963(12)	13.2994(17)	19.242(4)
α	90	94.159(11)	89.228(2)	90	71.351(5)	90
β	103.480(3)	90.51(2)	75.765(2)	100.925(3)	84.932(5)	100.518(11)
γ	90	104.78(4)	70.977(2)	90	78.919(5)	90
V/Å^3	2009.8(2)	1679(5)	1080.00(8)	2175.3(2)	1012.8(2)	2247.8(7)
Z	4	2	2	4	1	4
ρ_{cal}/ g cm^{-3}	1.489	1.469	1.662	1.650	1.564	1.859
μ/mm^{-1}	0.205	0.225	0.455	0.452	0.340	3.755
θ Range/°	1.96 - 20	2.00 - 20	1.79 - 30.56	1.86 - 27.72	1.62 – 22.5	1.86 - 27.83
Ref. (meas. / ind.)	5992/ 2942	17434/ 6529	30881/ 6607	38649/ 5083	15739/ 2948	62927/ 5308
Observed>2σ	2320	2898	4819	3284	1959	3937
Rint	0.0444	0.2110	0.0665	0.0920	0.1007	0.0952
Completeness %	95.7	95.0	99.8	99.4	98.2	99.4
Parameters	302	471	376	376	303	333
GooF	1.081	1.239	0.945	0.922	0.984	0.935
R_1 (obs)	0.0546	0.1739	0.0376	0.0397	0.045	0.0319
R_1 (all)	0.0721	0.2644	0.0586	0.0797	0.0896	0.049
wR2 (all)	0.1538	0.4876	0.0909	0.0762	0.1065	0.0785
$\rho_{max,min}$/e Å^{-3}	0.85, -0.365	0.947, -0.704	0.524, -0.320	0.474, -0.458	0.402, -0.365	1.092, -0.558

Notes and references

[a] Department of Chemistry, University of Bath, Bath, BA2 7AY, UK. Email: C.C.Wilson@bath.ac.uk

† The crystallographic details for **1-12** have been deposited with the Cambridge Structural Database, with CCDC numbers 984162-984173 Electronic Supplementary Information (ESI) available: crystal structure data and refinement information, details of hydrogen bonds and parameters, additional solubility curves. . See DOI: 10.1039/b000000x/

1. G. P. Stahly, Cryst. Growth Des., 2007, 7(6), 1007–1026.
2. A. V. Trask, Mol. Pharmaceutics, 2007, 4(3), 301–309.
3. N. Schultheiss and A. Newman, Cryst. Growth Des., 2009, 9(6), 2950–2967.
4. B. Kojic-Prodic and Z. Ruzic-Toros, Acta Crystallogr., Sect. B: Struct. Crystallogr. Cryst. Chem., 1982, 38(11), 2948–2951.
5. F. Vrecer, S. Srcic and J. Smid-Korbar, Int. J. Pharm., 1991, 68, 35–41.
6. J. F. Vrecer, M. Vrbinc and A. Meden, Int. J. Pharm., 2003, 256, 3–15.
7. A. R. Sheth, S. Bates, F. X. Muller and D. J. W. Grant, Cryst. Growth Des., 2005, 5(2), 571–578.
8. A. R. Sheth, S. Bates, F. X. Muller and D. J. W. Grant, Cryst. Growth Des., 2004, 4(6), 1091–1098.
9. C. Wales, L. H. Thomas and C. C. Wilson, CrystEngComm, 2012, 14, 7264–7274
10. K. Naelapää, J. van de Streek, J. Rantanen and A. D. Bond, J. Pharm. Sci., 2012, 101(11), 4214-4219.
11. K. Fucke, S. A. Myz, T. P. Shakhtshneider, E. V. Boldyreva and U. J. Griesser, New J. Chem., 2012, 36, 1969-1977.
12. J. Bordner, P. D. Hammen and E. B. Whipple, J. Am. Chem. Soc., 1989, 111, 6572–6578.
13. J. M. Geckle, D. M. Rescek and E. B. Whipple, Magn. Reson. Chem., 1989, 27(2), 150-154.
14. S. L. Childs and K. I. Hardcastle, Cryst. Growth Des., 2007, 7(7), 1291–1304.
15. H. A. Cheong and H. K. Choi, Pharm. Res., 2002, 19 (9), 1375 - 1380
16. S. L. Johnson and K. A. Rumon, J. Phys. Chem., 1965, 69(1), 74–86.
17. B. R. Bhogala, S. Basavoju and A. Nangia, CrystEngComm, 2005, 7, 551-562.
18. S. L. Childs, G. P. Stahly and A. Park, Mol. Pharmaceutics, 2007, 4(3), 323-338.
19. D. M. Cristancho, D. R. Delgado, A. R. Holguin, F. Martinez and R. G. Sotomayor, J. Molec. Liquids, 2013, 180, 34–38.
20. J. A. Cordero, L. Alarcon, E. Escribano, R. Obach and J. Domenech, J. Pharm. Sci., 1997, 86(4), 503–508.
21. G. M. Sheldrick, Acta Crystallogr., Sect. A: Found. Crystallogr., 2007, 64, 112–122.
22. L. J. Farrugia, J. Appl. Crystallogr., 1999, 32, 837–838.
23. S.S. Kumar and A. Nangia, Cryst. Growth Des., 2014, 14, 1865-1881.

